energies

MDPI

Article

Performance Analysis of Thermal Image Processing-Based Photovoltaic Fault Detection and PV Array Reconfiguration—A Detailed Experimentation

Srinivasan Alwar [1], Devakirubakaran Samithas [2], Meenakshi Sundaram Boominathan [1], Praveen Kumar Balachandran [3] and Lucian Mihet-Popa [4,*]

[1] Department of Electrical and Electronics Engineering, Sethu Institute of Technology, Virudhunagar 626115, India
[2] Department of Electrical and Electronics Engineering, QIS College of Engineering and Technology, Ongole 523272, India
[3] Department of Electrical and Electronics Engineering, Vardhaman College of Engineering, Hyderabad 501218, India
[4] Faculty of Information Technology, Engineering and Economics, Oestfold University College, 1757 Halden, Norway
* Correspondence: lucian.mihet@hiof.no

Abstract: Due to the flexibility, sustainability, affordability, and ease of installation of solar photovoltaic systems, their use has significantly increased over the past two decades. The performance of a solar PV system can be constrained by a variety of external conditions, including hotspots, partial shade, and other minor faults. This causes the PV system to permanently fail and power losses. The power output in a partially shaded solar system is improved in this work by the introduction of a fault classifier based on thermal image analysis with a reconfiguration algorithm. For that purpose, the entire PV array is divided into two parts, with one of these being the male part and the other being the female part. MOSFET switches are used to build the switching matrix circuit that connects these parts. The Flir T420bx thermal camera captures thermal pictures, and MATLAB/Simulink® is used to extract the image properties. The pairing reconfiguration pattern is found using an algorithm based on image processing and the image attributes. The switching signals to the switching circuit are triggered by an Arduino controller. The image attributes of the thermal images may also be used to categorize PV system defects. This reconfiguration technique is easy, simple to use, and it can also be used to check the health of each PV module. The performance of the proposed work was validated using a 5 kW PV system with a 4 × 5 TCT array configuration at Sethu Institute of Technology's renewable energy lab in India. The proposed method was simulated using the MATLAB-Simulink software program, and the outcomes were verified on different hardware setups.

Keywords: image processing; reconfiguration; photovoltaics; mean; standard deviation; MOSFET

Citation: Alwar, S.; Samithas, D.; Boominathan, M.S.; Balachandran, P.K.; Mihet-Popa, L. Performance Analysis of Thermal Image Processing-Based Fault Detection and Reconfiguration Algorithm in Partially Shaded PV Systems—A Detailed Experimentation. *Energies* **2022**, *15*, 8450. https://doi.org/10.3390/en15228450

Academic Editors: Athanasios I. Papadopoulos and Andrea Reverberi

Received: 26 September 2022
Accepted: 8 November 2022
Published: 11 November 2022

Publisher's Note: MDPI stays neutral with regard to jurisdictional claims in published maps and institutional affiliations.

1. Introduction

The world's energy demand and the rate at which traditional energy sources are being used up have both risen in recent decades and will continue to do so. If this phenomenon persists, conventional energy sources will no longer be accessible in the future. In order to maintain the equilibrium between energy demand and power supply, the energy need necessitates an alternate path for the energy sources. Utilizing renewable energy sources such as solar, wind, biomass, tidal energy, and others are needing a better way to maintain the balance between energy demand and power supply. The ecosystem is not harmed by renewable energy sources, which are abundant in nature. These sources are

not always available during harvest, yet they nonetheless produce a consistent overall result. Renewable energy sources are now expected to overtake other energy sources because of advancements in harvesting technology. In terms of easy setup, operation, low maintenance, and other factors, solar energy harvesting offers several benefits over other renewable energy sources. Based on the photovoltaic effect, solar photovoltaic systems convert sunlight (and the photons contained within) into direct electricity [1,2].

The first solar photovoltaic modules, with an energy conversion rate of 6.33 percent, were introduced to the energy market in 1981. Compared to other renewable energy sources, the PV system's installation has fewer drawbacks. While the current generated by a PV cell is directly proportional to the amount of solar radiation received by the PV cell surface, the power generated by a PV system depends heavily on solar radiation [3]. On the other hand, a variety of factors, some of which are diagnosable, such as partial shade, hotspots, diode failure, minor flaws, fractures, the burning of strings, PV cell failure, and others, restrict the amount of power that a PV system can produce. However, certain factors, such as hotspots and partial shading, are unavoidable [4]. PV systems commonly experiences partial shade, which is the most prevalent occurrence. The uneven distribution of solar irradiation caused by this partial shade reduces power output by creating hotspots that raise the temperature of the PV panel. Additionally, due to the excessive current flow, this causes the PV cell to fail. The building-integrated PV system is more affected by partial shade. To increase the power conversion rate of a PV system, the effect of partial shade must be reduced. There are several strategies available to lessen the effects of partial shadowing. By obtaining the GMPP (global maximum power point), as explained in [5], maximum power point tracking (MPPT) can be one of the approaches that creates an equilibrium between the source resistance and load resistance. Conventional MPPT approaches, such as MPPT algorithms based on perturb and observe (P&O) [6] and incremental conductance (InC) [7], may fail to acquire the GMPP in a complicated partial shading situation because of the high cost of MPPT implementation on PV systems. Optimization techniques that make use of particle swarm optimization (PSO), neural networks (NNs), artificial neural networks (ANNs), ant colony optimization (ACO), the cuckoo search-based algorithm [8], and the musical chair-based algorithm [9] are integrated with conventional methods. The ability to precisely of produce the GMPP is slowly improving because of these strategies.

PV array configurations can also reduce the impact of partial shadowing by distributing light equally over the array. In the beginning, two array configurations were used: series (S) and series-parallel (Se-P). In certain situations, a complex type of partial shading may cause the available power output at the load terminal to be zero. In [10], the total-cross-tied (TCT) array configuration, which combines both series and series-parallel array design, was created. Although the TCT method lessens the impact of partial shade, it was ineffective in particular shading patterns. For increasing the power production, several PV array arrangements such as honeycomb, bridge-connected, and Sudoku pattern array configurations were discussed in [11]. The reconfiguration technique [12] is another method for reducing partial shadowing. In this method, the interconnections between the PV modules are switched based on the partial shading situation. The two types of reconfiguration procedures are static reconfiguration and dynamic reconfiguration. The reconfiguration strategy raises the cost of a PV system by requiring many sensors, switches, controlling units, and cables. Time is set aside during reconfiguration to measure the data and rearrange the interconnections of the modules. As mentioned before, the reconfiguration technique is highly complicated due to the numerous measurements, scanning time, and pattern construction time involved. The reconfiguration technique is the focus of much research aimed at reducing the amount of data needed, the scanning time, and the complexity.

The scanning pattern reconfiguration technique in [13] requires electrical data such as the current and voltage as well as values for temperature and radiation. This approach requires a longer scanning period, which is even shorter in [14]. The drawbacks have been

solved by the suggested reconfiguration procedure, which effectively increases power production. Injecting the compensatory current across the shaded or defective PV rows is known as the current injection approach, and other techniques were presented in [15]. By operating the PV system with even current generation rows, the mismatch losses are greatly reduced, and the power produced is increased.

For minimizing the impact of partial shadowing in a PV system, further configurations derived from puzzle patterns were explored in spiral pattern reconfigurations [16] and both L-Shape propagating array [17] and KenKen puzzle [18] configurations. When developing any type of system, it is essential to consider fault detection and diagnosis equipment [19]. The energy production, transmission, and distribution units require extra attention. There are several approaches for finding faults in solar photovoltaic systems. The misidentification of issues might cause a PV system serious harm. Due to an undetected diode failure or burning on the string, a PV module might malfunction permanently. A defect detection approach based on electrical factors was suggested in [20]. Early on, each PV string's performance is assessed to detect any abnormalities regarding the PV system.

Later, measurements based on PV generating units are performed, and a thorough report is produced for each unit. This includes information on power generation in relation to the available radiation, power generation in relation to the temperature of the environment, a comparison of the neighboring producing units, and efficiency. The variance in these statistics reveals the proportion of faults in the PV system. The assessment in digital contexts lays the foundation for defect identification via image processing. In [21], the authors proposed employing resistance analysis by mapping of potential (RAMP) methods to map contact resistance (CoRRescan) and locate shunts on solar cells. Both reducing contact resistance losses and measuring contact resistance are crucial.

The fine structure of solar cells with and without metallic coatings may be examined using a scanning electron microscope (SEM) and atomic force microscopy (AFM) images, allowing for rapid and simple structural analysis, according to a novel approach presented in [22]. The local photo-response of a solar cell may be determined using the light beam-induced current (LBIC) approach, allowing for the evaluation of the spatial distribution of electrical characteristics and defects. In [23], the I–V characteristics, short-circuit current, carrier lifespan, and quantum efficiency of a solar cell were measured while the beam probe was being moved over a solar cell. The use of thermography image on the PV fault detection [24], MPPT techniques [25], temperature distribution analysis [26] were discussed.

The main contributions of this research paper are as follows:

- A novel defect classifier with dynamic reconfiguration based on thermal image processing is proposed.
- The power output in the partially shaded solar system is improved by the introduction of a fault classifier based on thermal image analysis with the reconfiguration algorithm.
- The pairing reconfiguration pattern is found using an algorithm based on image processing and the image attributes.
- The performance of the proposed work was validated first using the MATLAB-Simulink software package and then using an experimental setup featuring a 5 kW PV system with a 4 × 5 TCT array configuration.

The article is structured as follows: Section 2 explains how the reconfiguration algorithm was created; Section 3 explains how the pairing reconfiguration was experimentally validated; Section 4 explains how a fault classifier based on thermal image processing was created; and Section 5 explains how the thermal image processing-based pairing reconfiguration algorithm was validated.

2. Pairing Reconfiguration Algorithm

In a conventional TCT PV array, the current generation of each row should be almost equal; otherwise, current match will occur between the PV rows, causing a mismatch power loss on the PV system, which is when the minimum current generating rows limit the entire power generation. Therefore, it is important to operate the PV rows with an even current generation. The proposed pairing reconfiguration algorithm makes all PV rows as an even current generating row. This will reduce the mismatch losses, so that the power output can be enhanced. Initially, the PV system is split into two parts named male and female. Both the male and female parts must have an equal number of rows. These parts are connected through the switching matrix circuit, where the connections are established by the pairing reconfiguration algorithm. The pairing pattern of the algorithm is obtained based on the current generating capability of the PV rows. The maximum current generating row from the male part is paired with the minimum current generating row of the female part. The main constraint of the proposed pairing reconfiguration algorithm is that at any instant of time one row from the male part is connected to only one row of the female part, but not more than one.

Depending on the current generation, males and females are categorized and then paired to achieve optimum power generation. The healthier part, male or female, is ranked as 1 in the sorting process. In Figure 1, M1, M2, M3, and M4 are the rows of the male part, and F1, F2, F3, and F4 are the rows of female part. The health of M1 is good compared to M2, the health of M2 is good compared to M3, and the health of M3 is good compared to M4. The health of F2 is good compared to F4, the health of F4 is good compared to F1, and the health of F1 is good compared to F3. For this group, the couples should be matched as M1–F3, M2–F1, M3–F4, and M4–F2, to achieve the best generation. The couple matching algorithm has been executed in this way by connecting the maximum current generating row of the male part with the minimum current generating row of the female part. This kind of couple matching results in almost equal health conditions in terms of the generations of the couples.

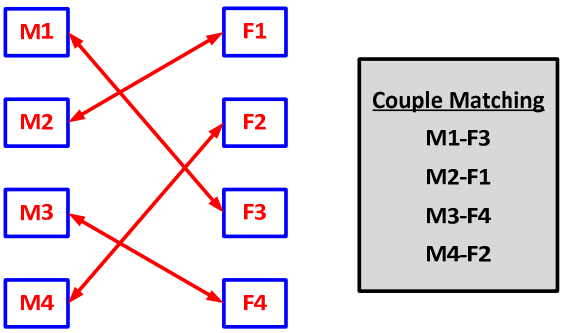

Figure 1. Male and female couple matching.

The Figure 2 shows the proposed 4 × 5 TCT array system for implementing the pairing reconfiguration algorithm.

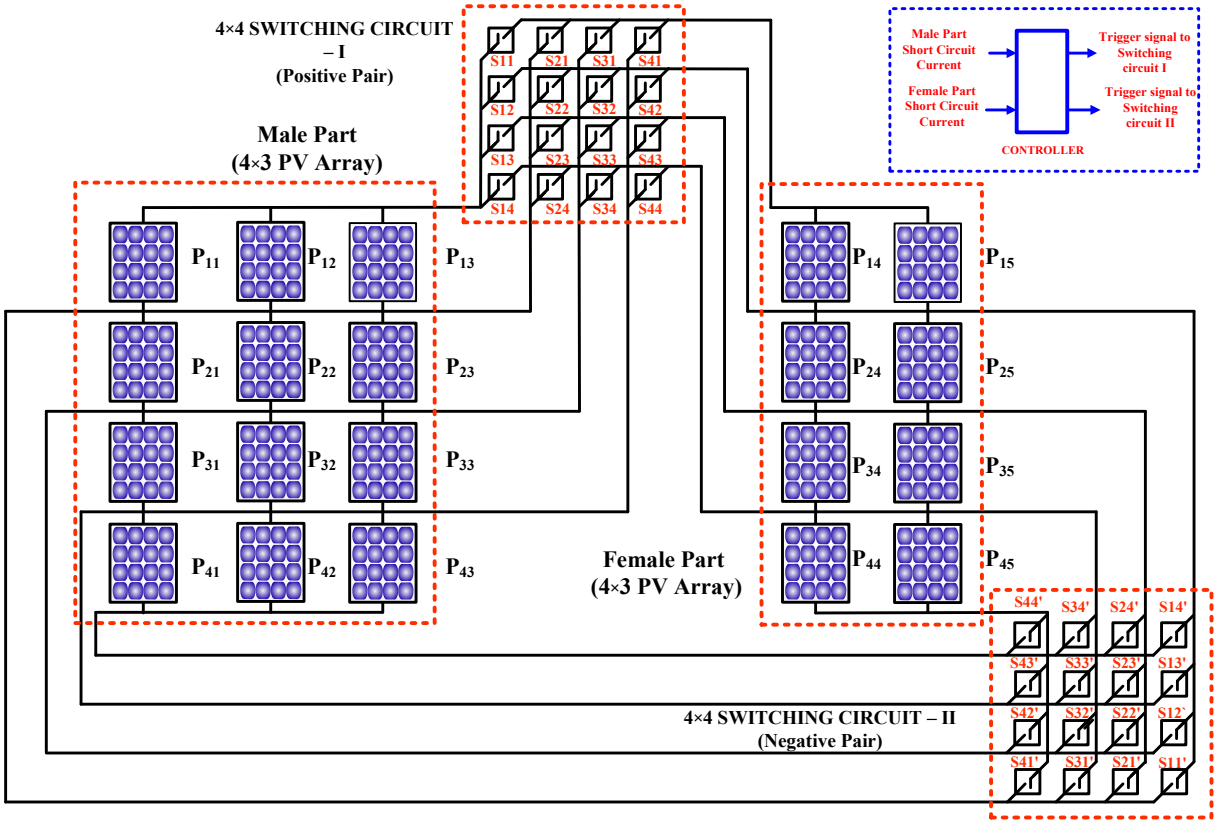

Figure 2. Proposed 4 × 5 TCT array with twenty panels.

The 4 × 5 TCT array can be split into a 4 × 3 male part and a 4 × 2 female part, and so, the male part has four males and female part has four females. Figure 3 shows the flowchart of the proposed method. Initially, the load current is measured, and after five seconds, the load current is measured again, before the percentage change in current (% ΔI_L) is calculated by Equation (1).

$$\%\Delta I_L = \frac{I_{L1} - I_{L2}}{I_{L1}} \times 100 \quad (1)$$

The working of the proposed methodology is represented as a flowchart, as shown in Figure 3. Under daytime normal conditions, the load current gradually increases in the morning and then decreases in the afternoon. During partial shading, the load current suddenly decreases (more than 5% within a fraction of a second). This helps to identify the partial shading period. In the pairing reconfiguration algorithm, if the first condition is satisfied (if the percentage change in the load current exceeds five percent), then the panels are reconfigured. The change in load current is calculated after the time period ΔDt (the delay time). In this paper, the value for ΔDt is taken as five seconds. To find the reconfiguration pattern, first, this algorithm disconnects the load away from the array and measures the short circuit current of each male in the male part and each female in the female part. Then, according to the values of their short circuit current, males and females are sorted (in descending order). Finally, a reconfiguration pattern is obtained by using Equation (2) and implemented by operating the matrix switching circuit accordingly. The matrix switching circuit has 16 switches for positive side control and 16 switches for negative side control. The matrix switching circuit can connect any female to any male, as described by the Equation (2).

$$\mathrm{Re}\,confguration\_Pattern(RC) = \begin{bmatrix} M_{SS1} & F_{SSX} \\ M_{SS2} & . \\ . & . \\ . & F_{SS2} \\ M_{SSX} & F_{SS1} \end{bmatrix} \quad (2)$$

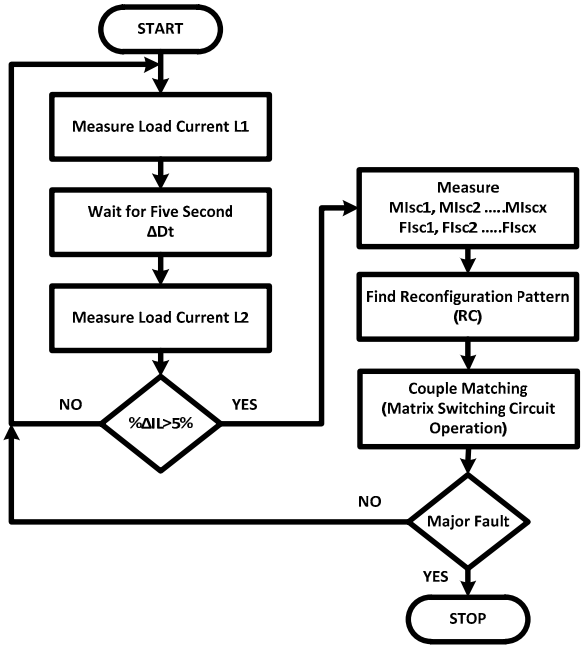

Figure 3. Flow chart of the proposed algorithm.

3. Experimental Setup Description

A 5-kW solar plant was installed in the Department of Electrical and Electronics of Sethu Institute of Technology, India and the specification of the PV panel are given in table 1. The rated capacity of the plant is 5 kW, and it was constructed by using twenty numbers of 250 W mono-crystalline PV panel, as shown in Figure 4. The array size of the PV array is 4 × 5, which can be split into 4 × 3 male parts and 4 × 2 female parts or 4 × 2 male parts and 4 × 3 female parts.

Figure 4. 5 kW PV Array.

The panel rating is given below.

Table 1. Specifications of PV panel.

S.No	Parameters	Specification
1	Maximum Power of a Single Panel (P_{OUT})	250 W
2	Open Circuit Voltage (V_{OC})	37.23 V
3	Short Circuit Current (I_{SC})	8.95 A
4	Maximum Voltage (V_M)	29.7 V
5	Maximum Current (I_M)	8.42 A
6	Tolerance (%)	±5%
7	STC Temperature (T_{STC})	25 °C
8	Normal Operating Temperature (T_A)	45 °C
9	Temperature Coefficient (%/°C)	−0.43%/°C

For the execution of the project, the positive and negative terminals of each PV panel were brought into the Centre for Renewable Energy Systems Laboratory on the second floor of the department, where the image processing technique reconfiguration algorithm could be performed. The photograph of the hardware setup is shown in Figure 5.

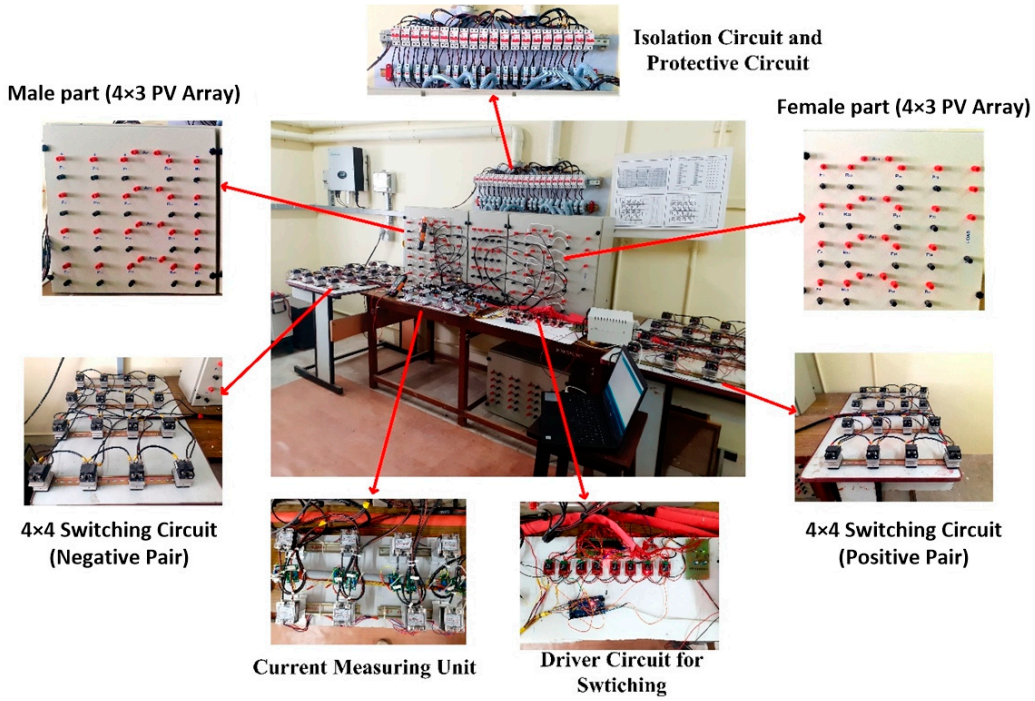

Figure 5. Photograph of the hardware setup.

Twenty positive and negative terminals of the PV modules were brought into the laboratory, as shown in the hardware setup. The hardware setup was initiated from the isolation circuit and protection circuit. If the system was to handle the high current flow of 30 A to 40 A of DC, it was necessary to provide the proper isolation and protective setup for avoiding electrical hazards. Therefore, the PV terminals were brought into the testing panel via the isolator and OLR (overload protective relay). The isolator circuit provided complete control over each PV module. During the wiring and interfacing of the measurement units, the power output from the modules can be turned off by the isolators. It is challenging work to interface any measuring units or switches or wires on active PV systems because it may damage the equipment, components, or the PV modules and sometimes it causes a fire accident. Such a protective step allowed for the completion of the testing and measurements in the PV system without any difficulties. Twenty 60 A, 2Pole isolators were used for the isolation circuit, and twenty 20 A DC cartage fuses with

cartages were used for the protective circuit. The positive and negative terminals of each PV module were connected to the testing panels through the isolation circuit and protective circuit.

At this stage, each module was ready for the integration of the experimental setup. A testing panel was fabricated for the project execution. This testing panel allowed for the easy interfacing of the necessary units, such as measuring units or switching units, with the 5 kW PV system, and the array configuration of the PV system could be changed in a desired manner, such as in a series-parallel (SE-P), total-cross-tied (TCT) or Sudoku puzzle pattern, etc.

For executing the couple matching algorithm, the inputs to the controller must be obtained appropriately. The short circuit current of each male part and female part is the input for the controller, which is measured by the current sensing unit, as shown in Figure 6. The R_{11}, R_{12}, R_{13}, R_{14}, R_{21}, R_{22}, R_{23}, and R_{24} are the solid-state relays, which are terminals that are connected across each row of male and female parts for shorting the male parts and female parts. A_{M1}, A_{M2}, A_{M3}, and A_{M4} are the current sensors connected across male parts and A_{F1}, A_{F2}, A_{F3}, A_{F4} are the current sensors connected across female parts. During the enabling time of the relays, the sensors measured the short circuit and stored it for the pairing reconfiguration algorithm. The short circuit period was 2 s and it was opened after this time.

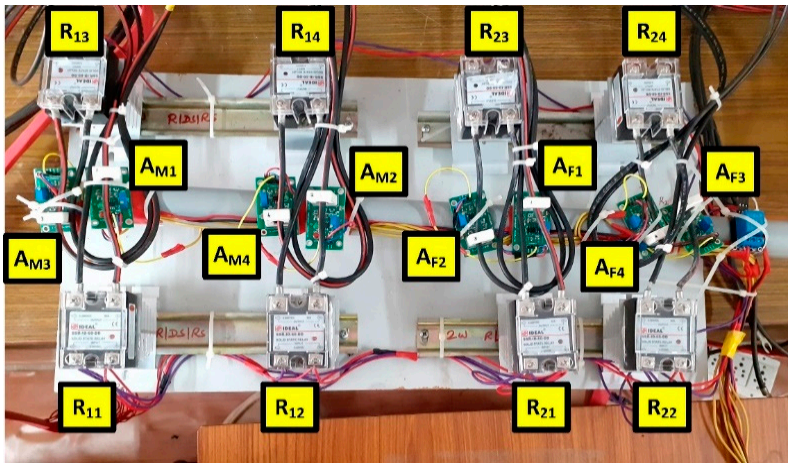

Figure 6. Photograph of current sensing unit.

The switching circuit was constructed with MOSFET for coupling the male part with the female part. The switching circuit size for any kind n×m PV array will be (2 × n × n) where n is the number of rows. In this work, the required number of switches was 32 (2 × 4 × 4) for the 4 × 5 PV array. The switching configuration is shown in the Figure 7a,b. The working principle of this circuit is to connect any one of the male part rows with any one of the female part rows. The layout diagram and a photograph of the switching matrix circuit are shown in Figure 7c.

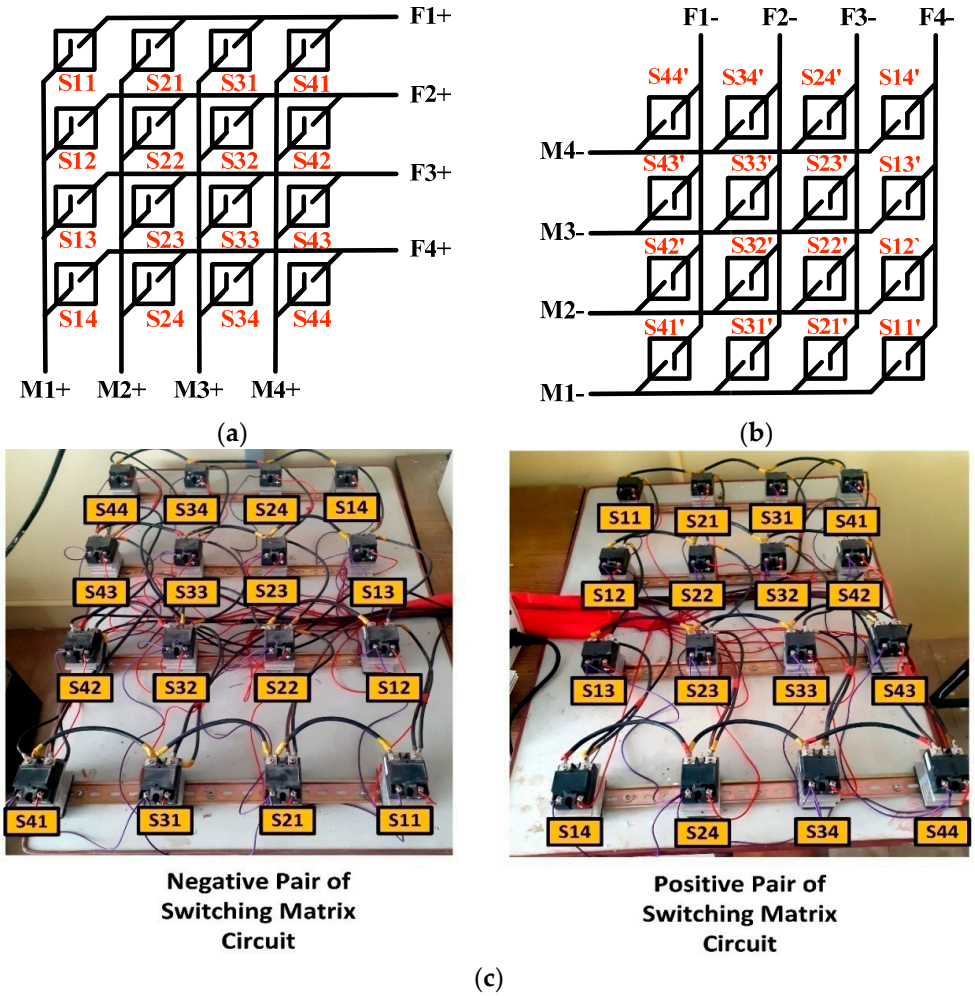

Figure 7. (**a**) Positive pair of switching matrix circuit; (**b**) negative pair of switching matrix circuit; (**c**) photograph of the switching matrix circuit.

The switching representation is given below in Table 2.

Table 2. Details of switching circuit.

S.No	Switch Name	Operation
1	S11, S11′	Connects Row 1 with Row 1
2	S12, S12′	Connects Row 1 with Row 2
3	S13, S13′	Connects Row 1 with Row 3
4	S14, S14′	Connects Row 1 with Row 4
5	S21, S21′	Connects Row 2 with Row 1
6	S22, S22′	Connects Row 2 with Row 2
7	S23, S23′	Connects Row 2 with Row 3
8	S24, S24′	Connects Row 2 with Row 4
9	S31, S31′	Connects Row 3 with Row 1
10	S32, S32′	Connects Row 3 with Row 2
11	S33, S33′	Connects Row 3 with Row 3
12	S34, S34′	Connects Row 3 with Row 4
13	S41, S41′	Connects Row 4 with Row 1
14	S42, S42′	Connects Row 4 with Row 2
15	S43, S43′	Connects Row 4 with Row 3
16	S44, S44′	Connects Row 4 with Row 4

S represents connection from male to female; S′ represents connection from female to male.

The triggering pulse from the Arduino controller was not sufficient for operating the switching matrix circuit. So, a switching driver circuit was designed for amplifying the switching signals, as shown in Figure 8. There sixteen numbers relay drivers were used for operating the sixteen solid-state relays of positive and negative pairs of the switching matrix circuit. The rating of the SSR allowed for a 60 A DC current to be passed through it, and 3–32 V DC is the operating range of triggering pulses.

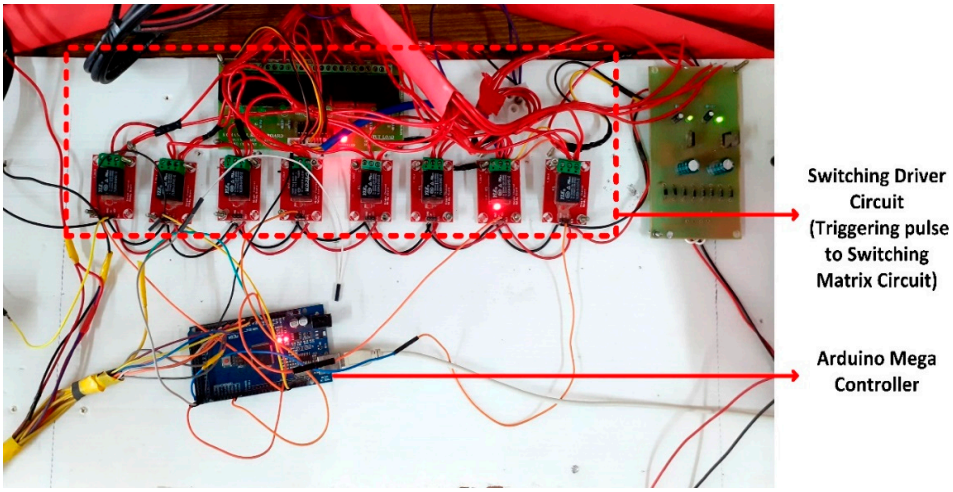

Figure 8. Photograph of switching driver circuit.

The couple matching algorithm-based reconfiguration method was implemented in the installed 5 kW PV system. All the required equipment, such as the current sensing unit, switching matrix circuit, protection, and isolation circuits, were related to the PV system. The shading patterns were created manually in the PV system using cardboard sheets.

The output analysis was carried out under the eight kinds of possible shading patterns, such as uneven row shading (UR), uneven column shading (UC), diagonal shading, random shading, short and narrow shading (SN), short and wide shading (SW), long and narrow shading (LN), and long and wide shading (LW). These are the most common shading patterns caused by nearby objects, trees, buildings, and clouds. The effectiveness of the proposed couple matching algorithm was analyzed under these shading patterns and validated with the other array configurations such as series-parallel and total-cross-tied configurations. The eight kind of shading patterns were applied on the PV system, as shown in Figure 9. The power output and short circuit current were measured and are given in Tables 3–5. The output comparison chart is shown in Figure 10.

Table 3. Output Power of Series-Parallel Array Configuration.

S. No	Shading Type	Series-Parallel Configuration			
		Simulation		Experimental	
		I_{SC} (A)	P_{OUT} (Watts)	I_{SC} (A)	P_{OUT} (Watts)
1	UR	35.8	4001	33.1	3691
2	UC	25.1	2633	23.6	2662
3	Diagonal	23.3	2523	21.2	2394
4	Random	12.5	1330	11.4	1265
5	SN	30.9	3381	29.1	2317
6	SW	22.4	2501	20.6	2304
7	LN	14.3	1600	12.8	1539
8	LW	12.5	1432	10.9	1096

Table 4. Output Power of Total-Cross-Tied Array Configuration.

S. No	Shading Type	Total-Cross-Tied Configuration			
		Simulation		Experimental	
		I_{SC} (A)	P_{OUT} (Watts)	I_{SC} (A)	P_{OUT} (Watts)
1	UR	35.8	4001	32.9	3630
2	UC	25.1	2605	23.7	2649
3	Diagonal	29.5	3268	28.2	3134
4	Random	21.6	2305	20.1	2243
5	SN	30.9	3347	28.4	3168
6	SW	24.4	2899	21.8	2517
7	LN	17.9	2040	16.3	1895
8	LW	16.1	1826	14.5	1686

Table 5. Output Power of Proposed Method.

S. No	Shading Type	Couple Matching Algorithm Based Reconfiguration					
		Simulation			Experimental		
		I_{SC} (A)	P_{OUT} (Watts)	% ΔI_L	I_{SC} (A)	P_{OUT} (Watts)	% ΔI_L
1	UR	35.8	4001	20.0%	33.2	3711	17.0%
2	UC	31.3	3361	30.1%	28.7	3207	28.3%
3	Diagonal	34.5	3793	22.9%	32.6	3631	18.5%
4	Random	26.4	2818	41.0%	25.1	2817	37.3%
5	SN	35.8	3914	20.0%	31.8	3554	20.5%
6	SW	29.5	3303	34.1%	26.9	2998	32.8%
7	LN	25.9	2898	42.1%	24.3	2735	39.3%
8	LW	21.5	2432	52.0%	18.7	2096	53.3%

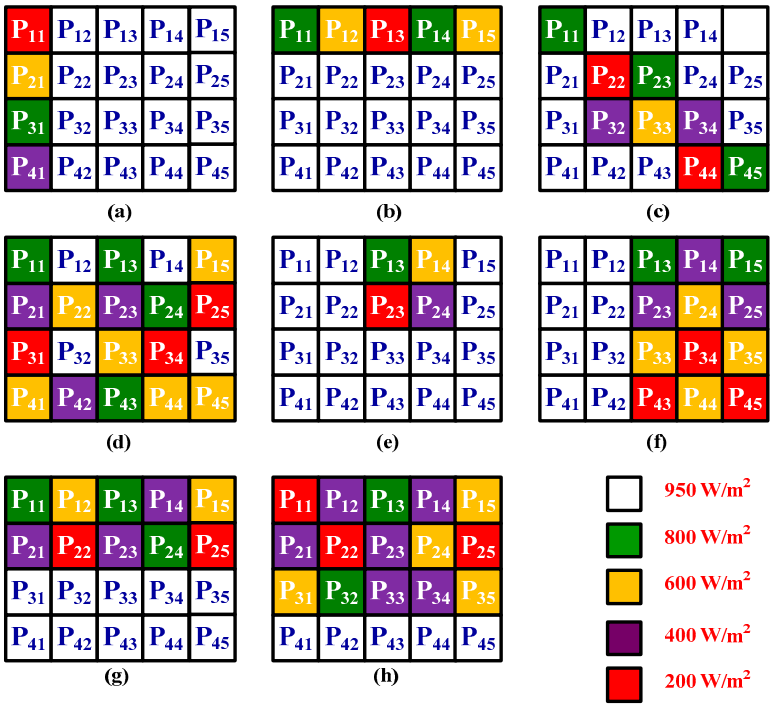

Figure 9. (**a**) Uneven row shading; (**b**) uneven column shading; (**c**) diagonal shading; (**d**) random shading (**e**) short and narrow shading; (**f**) short and wide shading; (**g**) long and narrow shading; (**h**) long and wide shading.

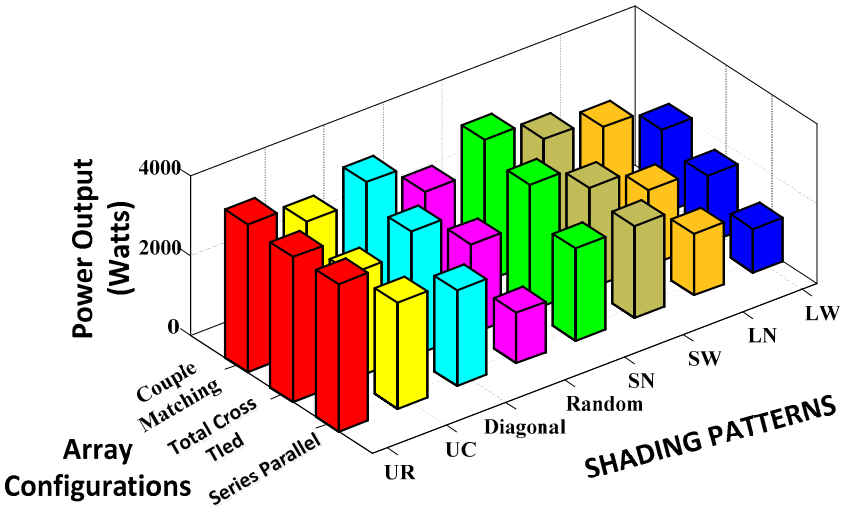

Figure 10. Comparison chart of output power.

By comparing the power output of existing and proposed methods, the proposed pairing reconfiguration scheme generates maximum power. In the context of uneven row shading, the power output of all methods is nearly the same because the shade dispersion is similar in all methods. In uneven column shading patterns, the dispersion of shading in the proposed method made a difference in the power output. The couple matching algorithm reconfigures the shaded column to uniformly disperse the shading as much as possible in the PV array. In the context of diagonal shading patterns, the TCT configuration disperses the shading more than the Se-P configuration, but the proposed method is superior to the TCT in shade dispersion and power generation. In a random shading pattern, an uneven shading is spread over the PV array. The Se-P array configuration generates very low power due to the high mismatch loss due to the shading. The TCT disperses the shading more than the Se-P but failed to extract maximum power from the PV array. The pairing reconfiguration algorithm disperses the shading as much as possible in the PV array by reconfiguring the shaded PV modules and extracts maximum power from it. In short and narrow, short and wide, long and narrow, and long and wide shading patterns, the effectiveness of the reconfiguration algorithm is increased. The reconfigured PV system extracts high power from the PV array, which is almost two times greater than when using existing methods. The main reason behind the effectiveness of the proposed work is the dispersion of shading levels. The reconfigured PV array highly disperses the shading over the PV array, which reduces the mismatch losses and enhances the power output. The pairing reconfiguration algorithm is an effective and simple PV system approach for maximum power extraction.

4. Implementations of the Image Processing Technique and Results

For the image processing techniques, the Flir T420bx thermography camera (USA) was used in this work. It is necessary to capture thermal images with a clear top view so that the image processing process can be carried out with more accuracy. The 5 kW PV system was installed on the rooftop of the institution with the proper clearance for receiving the solar irradiation. A 15m high lightning arrester was available near the PV system. For capturing the top viewed thermal image of the PV system, a setup was implemented on the tower of the lighting arrester, as shown in Figure 11.

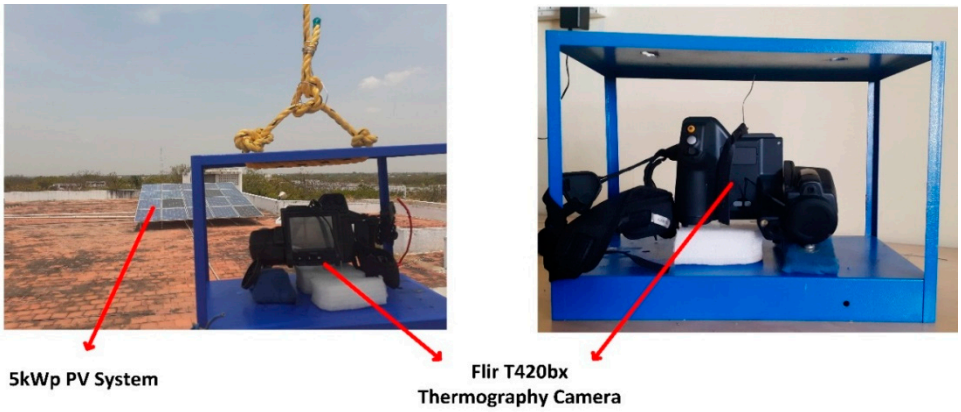

Figure 11. Photograph of thermal camera arrangements.

A wheel with rope and a camera base was fabricated in the lath of our institution. The thermal camera was placed in the camera stand with safe base, and this base was knotted with the wheel. Thanks to these arrangements, the camera could be placed at the top of the lightning arrester tower to capture the top view of the PV system. The thermal images could be captured through Wi-Fi or Bluetooth connectivity. These images were fed to the computer via Wi-Fi connectivity. The images were further fed to MATLAB/Simulink® for image processing. The individual images of each panel were cropped by the creation of a window and, the image features and attributes were extracted from each window. Image attributes, such as the mean, standard deviation, contrast, and entropy, were extracted for image processing and fault classification. For classifying the faults, a neural network (NN)-based fault classifier was used. The fault classifier was operated with three components, i.e., trained variables, testing variables, and classifying sets. Trained variables possess the data of known structures, classifying sets possess classification detail data, and trained variables to possess the image attribute data to be tested.

ANN is an information processing architecture inspired by biological nervous systems. The key element of this processing system is the neurons which are interconnected in large numbers. ANN's can be used to solve specific problems such as pattern recognition and data classification. The process structure of the feed-forward NN and the block diagram of the proposed image processing-based fault detection and reconfiguration algorithm are shown in Figure 12. ANN learns by example, and learning in biological systems involves adjustments to the synaptic connections that exist between the neurons.

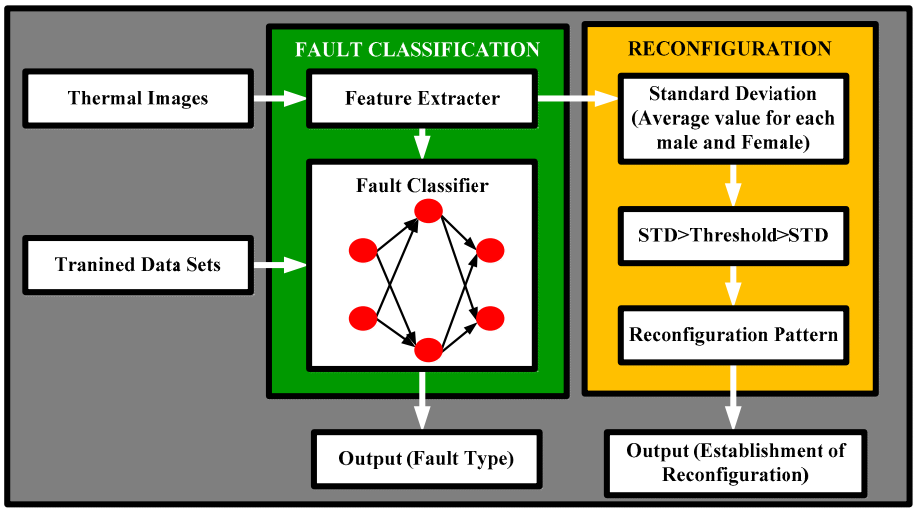

Figure 12. Block diagram of the proposed work.

The neural network has the two kinds of data sets, i.e., trained data sets (known data) and testing data sets (unknown data). In this work, the trained data set was obtained from thermal images of healthy PV modules and faulted PV modules. Under different irradiation conditions (from minimum to maximum), the thermal images were captured using the Flir T-420bx thermal camera. The features of the thermal images were extracted using an image processing tool in MATLAB. These features were fed to the neural networks as the trained data sets. These data sets had individual values such as healthy, shaded, cracked, partially shaded, hotspot, and delaminated PV modules. The training data set contained individual data for each kind of fault. Four image features were extracted from the thermal images and the features were mean, standard deviation (STD), entropy, and norm. The trained data were also considered the reference data for classifying faults. After the trained data set was obtained, fault classification details were given to the neural network. The trained data possess the details of various faults in the PV system, and when the testing input carries the unknown detail to the classifier, it then adjusts its weights, and the classifier compares this with the trained and testing variables and classifies the input. For analyzing the performance of the proposed fault detection method, some faults were intentionally created on the PV array. This work was validated in the 4 × 5 PV array. In the PV array, dust and talcum powder were spread over the surface of the PV modules P12, P13, P14, P22, P23, and P24. In P33 and P44, the interconnections were reversed, so that the heat would be dissipated, creates the hotspot in this location. In the position of P35 and P45, the PV modules were replaced with four-years-old panels which were almost delaminated due t poor maintenance. The PV modules P42, P43, and P44 were completely shaded by cardboard sheets. and the PV modules P21 and P31 were partially shaded. The fault classification types are provided in Table 6. If the testing variable carries the data of a healthy module, then the classifier produces an output of 1, for shaded modules the output is 2, for partially shaded modules it is 3, for the cracked modules it is 4, for the modules with a hotspot it is 5, and for delaminated modules it produces 6.

Table 6. Fault classification details of NN.

S. No	Type of Panel	Classification Type
1.	Healthy	1
2.	Shaded	2
3.	Partially shaded	3
3.	Cracked	4
4.	Hotspot	5
6.	De-lamination	6

A flow chart of the image processing-based fault classification and reconfiguration algorithm is shown in Figure 13. A thermal image of the 5 kW PV system with various faults was captured by the Flir T420bx thermography camera, as is also shown in the figure. This image was processed using MATLAB, and each module was cropped by the creation of a window. Then, image features such as mean, standard deviation, entropy, and norm were categorized. These features were provided as testing variables to the neural network (NN)-based fault classifier. The neural network was already trained by the training data set so that it could easily classify the operating state of each panel. The neural network processed the trained and testing data, and it showed the operating state of each PV module. After the classification of the defects, the image features were fed to the controller. The individual windows of the thermal images were sorted according to the male part and female part. Then, the image features of the PV modules belonging to the male part 1 were added together. Based on the image features, the pairing reconfiguration algorithm found the best pairs to form couples for maximum power generation. Then, the controller generated the reconfiguration pattern and executed the pairing via the switching matrix circuit.

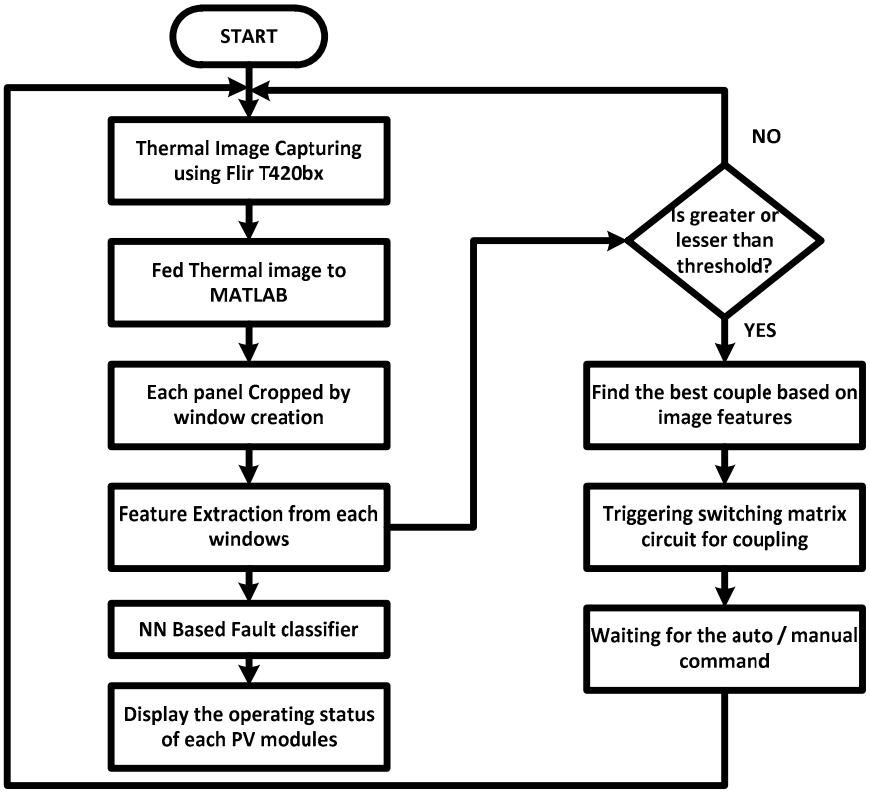

Figure 13. Flow chart of neural network-based fault classification with image processing-based reconfiguration.

Output Analysis of Image Processing Technique

Initially, defects such as shading, hotspots, delamination, and dust accumulation were created intentionally in the PV system, as shown in Figure 14. Each PV module had a different kind of defect so that it could be cross-validated using the image processing-based fault classification. The top view of the PV system was captured by the thermography camera. Certain kinds of faults such as hotspots, dust accumulation, and delamination could be viewed by the naked eye from the thermal images. However, to identify the exact defect and extract the defect details as digital data, the thermal images were fed into the computer, so that the image processing could be carried out. The image processing process extracts the attributes of every individual PV module and characterizes the operating state of each module, classifying it, for example, as healthy or defected. The fault classification and image processing process are provided below. The thermal image of the PV array was fed to MATLAB, which cropped each PV module by creating the windows, as shown in Figure 15. The excess area in each window of PV modules was suppressed based on an image's contrast features. The various steps involved in the image processing based fault classification has been represented as the block diagram as shown in Figure 16.

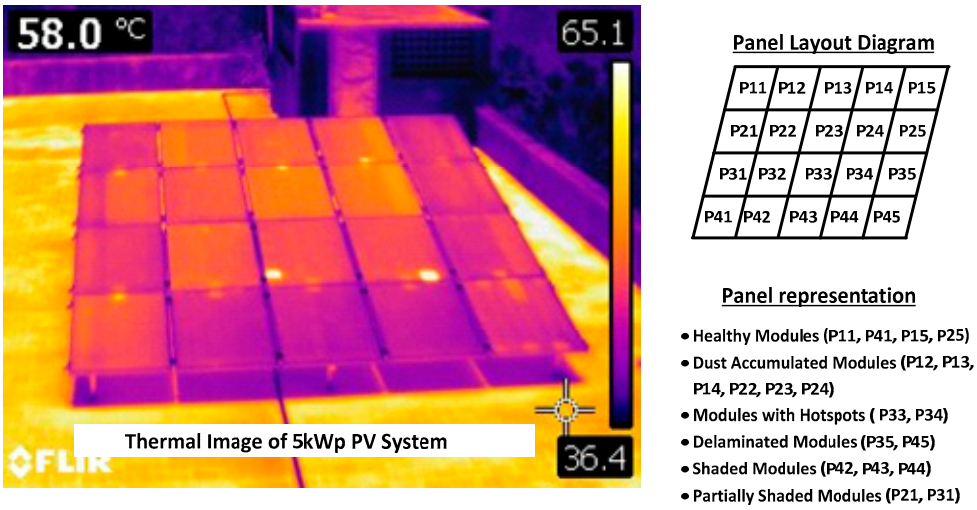

Figure 14. Thermal Image of 5 kW PV System with Various Defects.

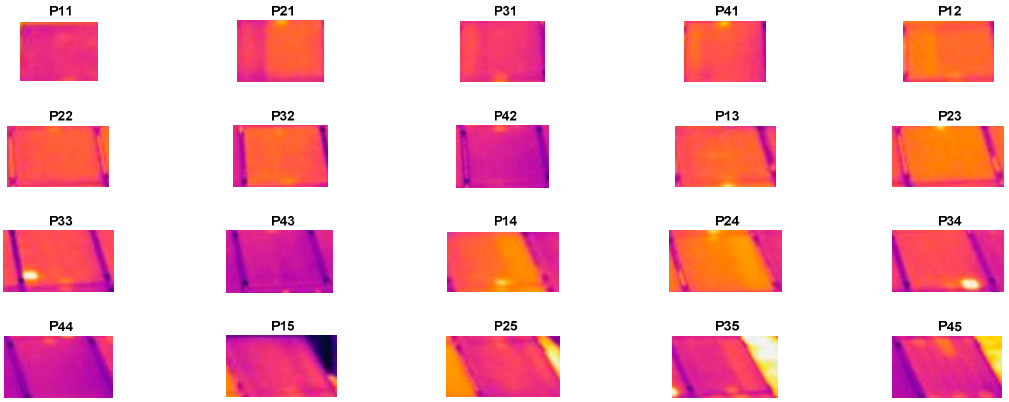

Figure 15. Window creation for each PV module.

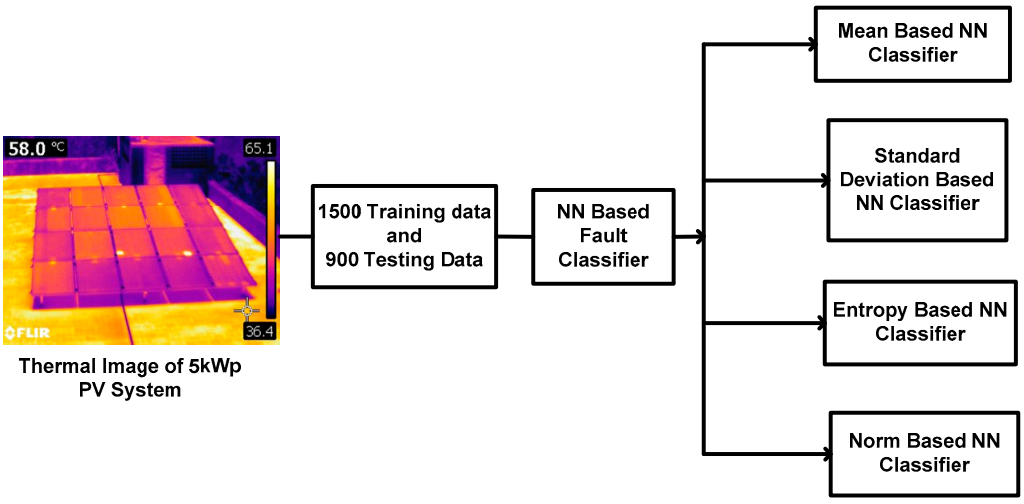

Figure 16. Steps in fault classification.

From each window, the necessary image features, such as the mean, standard deviation, entropy, and norm, were extracted. The neural network-based fault classifier was already trained with the 900 items of trained data. The trained data included details of the six defects. The trained data possessed 150 items of data on healthy modules, 150 items of data on shaded modules, 150 items of data on partially shaded modules, 150 items of data on cracked modules, 150 on hotspot-affected modules, and 150 on deaminated modules.

These data were already trained in the neural network-based fault classifier. From the figure of window creation, the image features were extracted. These features were fed into the neural network as the trained data, made up of 900 samples. The classifier uses the feed-forward back propagation neural network for the fault classification. This repeats the classification of each testing data until it is accurately classified.

The faults created on the PV array were randomly varied. Almost seventy-five kinds of different fault combinations were created on the PV array. For each fault combination, a thermal image was captured. Each thermal image was fed into the MATLAB tools for feature extraction. Thus, 150 samples of each fault condition were categorized and fed to the fault classifier. The NN-based fault classifier classified the testing data according to the trained variables. Based on the four features, the fault classification was obtained. The percentage of accuracy for each kind of image feature was validated. The accuracy can be obtained from the number of correctly and wrongly classified samples. The number of trained data and testing data which were correctly classified and the number of wrongly classified samples provide the percentage of accuracy, as given in Table 7.

Table 7. Comparison of various classifications during training.

Parameters	Image Features for Classification			
	Mean	**STD**	**Entropy**	**Norm**
Total no. of samples	900	900	900	900
Correctly classified	812	831	792	818
Total no. of 1	150	150	150	150
Total no. of 2	150	150	150	150
Total no. of 3	150	150	150	150
Total no. of 4	150	150	150	150
Total no. of 5	150	150	150	150
Total no. of 6	150	150	150	150
Classified samples				
1 as 1	135	139	139	136
2 as 2	138	136	131	143
3 as 3	143	134	127	141
4 as 4	137	139	130	135
5 as 5	127	143	129	131
6 as 6	132	140	136	132
Wrongly classified	88	69	108	82
Total % accuracy	90.22%	92.33%	88.00%	90.89%

There were 150 samples of each defect that were collected from the windows of thermal images. These data were further tested with the feed-forward back propagated neural network-based fault classifier with the trained variables. The classified outputs are displayed in Table 6. The accuracy of the classification was varied with respect to the feature-based classifier. A total of 150 samples of each defect were tested, and the classification details show the accuracy of the fault classification. The confusion matrix diagram of each fault classifier shows the number of correctly classified samples and the number of wrongly classified samples. The percentage of accuracy is shown in the confusion matrix diagram of Figure 17.

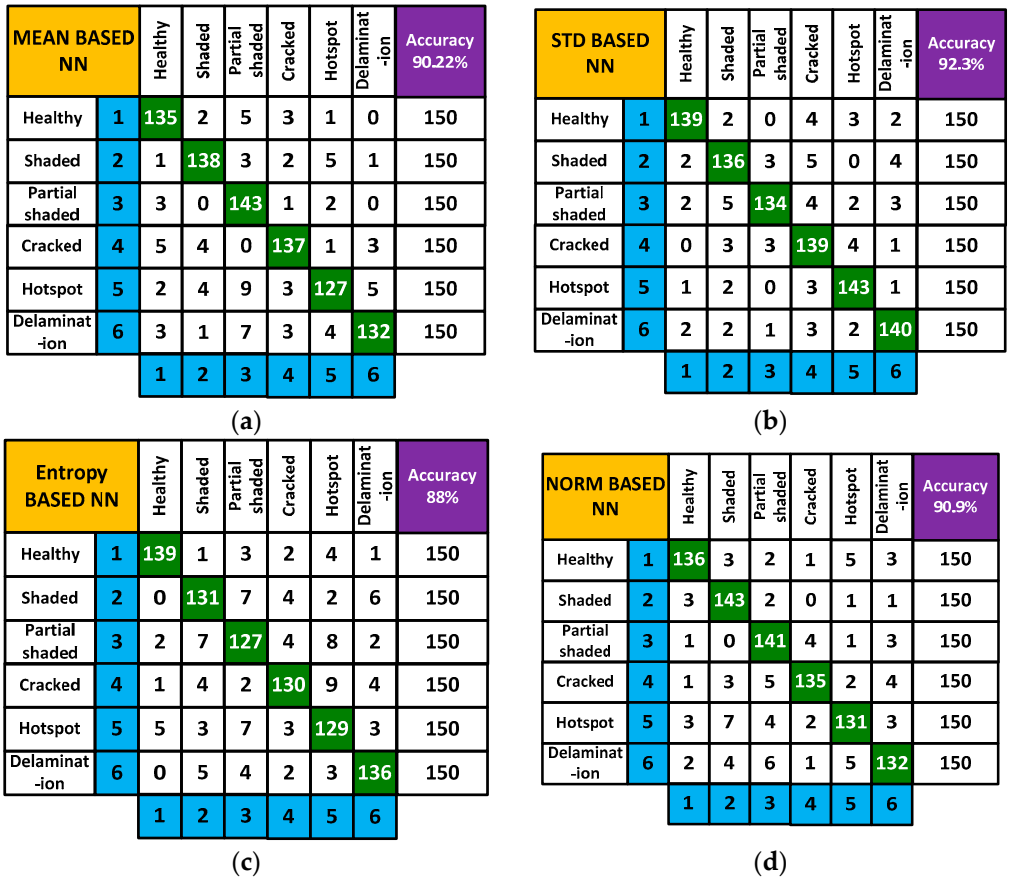

Figure 17. Confusion matrix diagram of (**a**) mean-based NN classifier, (**b**) standard deviation-based NN classifier, (**c**) entropy-based NN classifier, and (**d**) norm-based NN classifier.

5. Image Processing-Based Reconfiguration Method

The thermal image processing extracts the features of each PV modules, which is useful for obtaining the reconfiguration pattern. After achieving the fault classification, the controller initiates the reconfiguration process. If the controller found no faults in the PV system, the reconfiguration process will be skipped. Otherwise, the controller starts to find the image feature-based pairing reconfiguration pattern. The image features contain various details regarding the panel temperature variation in terms of mean, standard deviation, and entropy. The mismatch of losses in the PV system has a directly proportionality to the temperature variation between the PV cells. When the PV cell experiences defects such as partial shading or hotspots, the temperature will be raised. Normally, the faulted cell or module experiences a high temperature than healthy cells. The temperature difference can be identified by the controller using the image features. The mean and standard deviation shows the level of difference between the nearby cell and modules. Based on this data, abnormal PV modules in the PV system are identified. The controller possesses the details of each module's data. In the classification of faults, the standard deviation-based classification provides better accuracy compared to other features. Therefore, the standard deviation features were considered for the reconfiguration process. During window analysis, the standard deviation value for each panel was obtained. Concerning the reconfiguration pattern, a tolerance limit of ±10% was considered. If the tolerance level was lesser than ±10%, the PV module was operated in a healthy condition. For a normal healthy panel, 11.8869 was obtained as the threshold value. Additionally, ±1.18869 was chosen as the tolerance limit. If the standard deviation value was between 10.698 and 13.076, then the value of that corresponding panel was considered to be zero. If the obtained standard deviation value was greater than 13.076, then the threshold value was subtracted from the obtained value, and if the obtained value was lesser than 10.698,

then the obtained value has been subtracted from the threshold value. If the obtained value was between 10.698 and 13.076, then this value was considered to be zero. The above procedure was followed for each PV panel, and the obtained values were used for the reconfiguration process. For each male and female part, the obtained values were added, and the reconfiguration process was carried out. The sum of each male and female part were sorted in ascending order. The minimum value defines the minimum amount of fault presented in the system. Thus, the maximum value demonstrated that the male or female part has been affected with specific faults. After the sorting process, the male part with the lowest value was connected to the female part with the highest value. Thus, the male part with second lowest value was connected to the female part with second highest value. This process was continued until the male part with the highest value was connected to the female part with the lowest value. Thanks to this process, the pairing reconfiguration pattern as obtained. Based on the obtained pairing reconfiguration pattern, the controller generated the triggering signals to the switches and the switching matrix circuit established the reconfiguration. The power generation after the image processing-based reconfiguration is given in Table 8.

Table 8. Output power of image processing-based reconfiguration.

S. No	Shading Type	Paring Reconfiguration Algorithm				Accuracy
		Current Measurement Based		Image Processing Based		
		I_M	P_{OUT}	I_M	P_{OUT}	
		(A)	(Watts)	(A)	(Watts)	%
1	UR	31.2	3711	30.9	3671	98.9%
2	UC	27.0	3207	23.4	2780	86.7%
3	Diagonal	30.7	3631	29.7	3528	96.8%
4	Random	23.6	2817	23.4	2780	99.1%
5	SN	29.9	3554	27.3	3243	91.3%
6	SW	25.3	2998	24.7	2934	97.6%
7	LN	22.9	2735	19.6	2328	85.7%
8	LW	17.6	2096	17.3	2055	98.3%

The power generated by the image processing-based reconfiguration is given in Table 8. The image processing-based reconfiguration nearly achieves optimum couples with 90% accuracy in every case. This approach can generate more power than existing array configurations such as Se-P and TCT. In terms of UR, UC, diagonal, SN, and LN shading patterns, the image processing-based reconfiguration method achieves 98% accuracy with the current generation-based couple matching reconfiguration method. In terms of uneven column shading and long and narrow shading, this approach generates nearly 85% power , and this may be caused by the non-perfect matching of a couple. Perfect couples were achieved in terms of uneven row shading, diagonal shading, random shading, short and narrow shading, short and wide shading, and long and wide shading. The image processing-based reconfiguration approach achieved perfect couples in six kinds of shading patterns among eight, and the accuracy can be increased by repeated classification and iterations. An output power comparison chart comparing the image processing-based reconfiguration method and current measurement-based reconfiguration methods is provided in Figure 18.

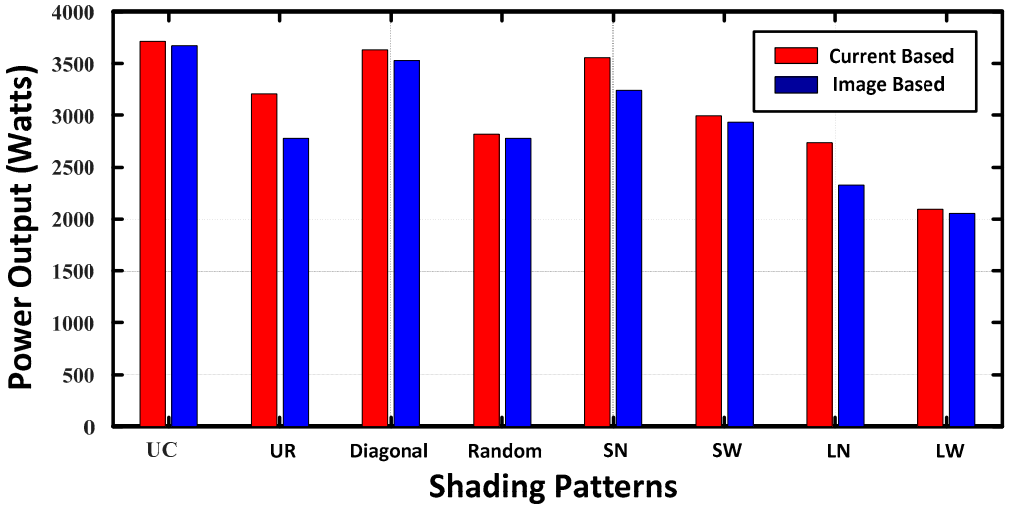

Figure 18. Comparison chart of output power.

The image processing technique was successfully achieved in real time. The fault classification result, along with the accuracy, and the image processing-based reconfiguration method with the power output were presented. The image processing technique provides a result with almost 90% accuracy in all cases of testing. This approach can be used for the any kind of electrical system for the fault classification, and it can be implemented without any additional setup. The image processing-based fault identification and classification method requires only a thermal image camera and image processing tools, and it does not require any additional measurements.

The accuracy of this method can be enhanced further by considering solar irradiance. In this work, we trained and tested the values based on the mean, standard deviation, entropy, and norm, which were obtained from the temperature values. This method provided efficient performance with regard to the obtainment of PV cell defects as well as in terms of reconfiguration. However, the measurement of irradiation can increase the efficiency of this method. The irradiance must be measured all day using a data logger. The irradiance values must be trained and tested according to the above classification procedure, providing improved performance.

The proposed thermal image processing-based fault classification process can be used for large power plants. Using the proper arrangements, it is possible capture the thermal images of every individual PV unit in a large PV plant. The thermal camera should capture the thermal images at regular intervals. An automated setup is required for operating the thermal camera, i.e., after capturing the thermal image of one PV unit, it should move on to the next unit until it reaches the last PV unit. After the completion of this cycle, it should start again in a cyclic process. Thus, the entire PV plant can be monitored regularly, and faults can be identified earlier. Furthermore, the reconfiguration method can be implemented in a unit-wise manner. This proposed method is feasible and can be implemented in real time applications.

6. Conclusions

The proposed pairing reconfiguration algorithm was successfully implemented in a 5 kW PV system. The performance of the proposed method was validated under all-possible shading patterns, and the proposed method performed better than the existing methods. The fault classification is performed by the neural network-based feed forward back propagated fault classifier. The fault classification is made possible by mean-, standard deviation-, entropy-, and norm-based image features. The accuracy of the fault classification was also confirmed, where the standard deviation-based fault classifier provided better accuracy. Furthermore, the thermal image processing-based reconfiguration is

developed from image features which are validated under all possible shading patterns. The performance of the electrical parameter-based pairing reconfiguration and thermal image processing-based reconfiguration were compared, where the thermal image processing-based reconfiguration provided the equivalent performance with the normal reconfiguration. There are no electrical measurements involved, but the isolation of panel connections is required in the thermal image processing-based pairing reconfiguration. This method is most useful for PV systems for health monitoring, as it successfully mitigates the consequences of partial shading and minor faults. The proposed work was successfully executed on a 4 × 5 PV array, and we plan to implement this work in a large PV power plant for the purpose of identifying the faults and reconfigure the PV system. This is a future work that the authors plan to execute.

Author Contributions: Conceptualization, D.S. and P.K.B.; Data curation, M.S.B.; Formal analysis, S.A., M.S.B. and L.M.-P.; Investigation, M.S.B. and L.M.-P.; Methodology, D.S. and P.K.B.; Software, D.S. and P.K.B.; Writing – original draft, D.S. and P.K.B.; Writing – review & editing, S.A. and L.M.-P. All authors have read and agreed to the published version of the manuscript.

Funding: This research received no external funding.

Data Availability Statement: Not applicable.

Conflicts of Interest: The authors declare no conflict of interest.

References

1. Serna-Garcés, S.I.; Bastidas-Rodríguez, J.D.; Ramos-Paja, C.A. Reconfiguration of Urban Photovoltaic Arrays Using Commercial Devices. *Energies* **2015**, *9*, 2.
2. Kumar, S.; Sharma, A.; Roy, B. Solar energy market developments in India. *Renew. Sustain. Energy Rev.* **2016**, *62*, 121–133. https://doi.org/10.1016/j.rser.2016.04.043.
3. Parida, B.; Iniyan, S.; Goic, R. A review of solar photovoltaic technologies. *Renew. Sustain. Energy Rev.* **2011**, *15*, 1625–1636. https://doi.org/10.1016/j.rser.2010.11.032.
4. Abdullah, M.; Mamun, A.; Selvaraj, J. Experimental investigation of the effect of partial shading on photovoltaic performance. *IET Renew. Power Gener.* **2017**, *11*, 912–921. https://doi.org/10.1049/iet-rpg.2016.0902.
5. Zhou, T.; Sun, W. Study on maximum power point tracking of photovoltaic array in irregular shadow. *Int. J. Electr. Power Energy Syst.* **2015**, *66*, 227–234.
6. Mohapatra, A.; Nayak, B.; Das, P.; Mohanty, K.B. A review on MPPT techniques of PV system under partial shading condition. *Renew. Sustain. Energy Rev.* **2017**, *80*, 854–867. https://doi.org/10.1016/j.rser.2017.05.083.
7. Podder, A.K.; Roy, N.K.; Pota, H.R. MPPT methods for solar PV systems: A critical review based on tracking nature. *IET Renew. Power Gener.* **2019**, *13*, 1615–1632. https://doi.org/10.1049/iet-rpg.2018.5946.
8. Eltamaly, A.M. An improved cuckoo search algorithm for maximum power point tracking of photovoltaic systems under partial shading conditions. *Energies* **2021**, *14*, 953. https://doi.org/10.3390/en14040953.
9. Eltamaly, A.M. A novel musical chairs algorithm applied for MPPT of PV systems. *Renew. Sustain. Energy Rev.* **2021**, *146*, 111135. https://doi.org/10.1016/j.rser.2021.111135.
10. Sai Krishna, G.; Moger, T. Optimal SuDoKu Reconfiguration Technique for Total-Cross-Tied PV Array to Increase Power Output under Non-Uniform Irradiance. *IEEE Trans. Energy Convers.* **2019**, *34*, 1973–1984. https://doi.org/10.1109/TEC.2019.2921625.
11. Pendem, S.R.; Mikkili, S. Modeling, simulation and performance analysis of solar PV array configurations (Series, Series–Parallel and Honey-Comb) to extract maximum power under Partial Shading Conditions. *Energy Rep.* **2018**, *4*, 274–287. https://doi.org/10.1016/j.egyr.2018.03.003.
12. Srinivasan, A.; Devakirubakaran, S.; Meenakshi Sundaram, B. Mitigation of mismatch losses in solar PV system - Two-step reconfiguration approach. Solar Energy. 2020, 206, 640–654. doi:10.1016/j.solener.2020.06.004.
13. Parlak, K. PV array reconfiguration method under partial shading conditions. *Int. J. Electr. Power Energy Syst.* **2014**, *63*, 713–721. https://doi.org/10.1016/j.ijepes.2014.06.042.
14. Murugan, M.S.; David, P.W.; Murugesan, P. Analysis of voltage/current mismatch in solar photovoltaic power plants during fault panel replacement. *Energy Sources Part A Recovery Util. Environ. Eff.* **2021**. https://doi.org/10.1080/15567036.2021.1909676.
15. Shakthivel, S.K.; David, P.W.; Backiyam, S.P.; Murugan, M.S. Square dynamic reconfiguration for the partial shaded photovoltaic system–simulation and experimental analysis. *Energy Sources Part A Recovery Util. Environ. Eff.* **2022**, *44*, 6868–6885. https://doi.org/10.1080/15567036.2022.2103215.
16. Cherukuri, S.K.; Balachandran, P.K.; Kaniganti, K.R.; Buddi, M.K.; Butti, D.; Devakirubakaran, S.; Babu, T.S.; Alhelou, H.H. Power Enhancement in Partial Shaded Photovoltaic System Using Spiral Pattern Array Configuration Scheme. *IEEE Access* **2021**, *9*, 123103–123116.

17. Srinivasan, A.; Devakirubakaran, S.; Sundaram, B.M.; Balachandran, P.K.; Cherukuri, S.K.; Winston, D.P.; Babu, T.S.; Alhelou, H.H. L-Shape Propagated Array Configuration with Dynamic Reconfiguration Algorithm for Enhancing Energy Conversion Rate of Partial Shaded Photovoltaic Systems. *IEEE Access* **2021**, *9*, 97661–97674.
18. Palpandian, M.; Winston, D.P.; Kumar, B.P.; Kumar, C.S.; Babu, T.S.; Alhelou, H.H. A New Ken-Ken Puzzle Pattern Based Reconfiguration Technique for Maximum Power Extraction in Partial Shaded Solar PV Array. *IEEE Access* **2021**, *9*, 65824–65837.
19. Wu, Z.; Hu, Y.; Wen, J.X.; Zhou, F.; Ye, X. A Review for Solar Panel Fire Accident Prevention in Large-Scale PV Applications. *IEEE Access* **2020**, *8*, 132466–132480. https://doi.org/10.1109/ACCESS.2020.3010212.
20. Silvestre, S.; da Silva, M.A.; Chouder, A.; Guasch-Murillo, D.; Karatepe, E. New procedure for fault detection in grid connected PV systems based on the evaluation of current and voltage indicators. *Energy Convers. Manag.* **2014**, *86*, 241–249. https://doi.org/10.1016/j.enconman.2014.05.008.
21. Van der Heide AS, H.; Schönecker, A.; Wyers, G.P.; Sinke, W.C.; Energy, E.S. Mapping of contact resistance and locating shunts on solar cells using Resistance Analysis by Mapping of Potential (RAMP) techniques. In Proceedings of the 16th European Photovoltaic Solar Energy Conference, Glasgow, UK, 1–5 May 2000; p. 1438.
22. González-Díaz, B.; González, J.F.G. SEM & AFM analysis for silicon-based solar cells. In *Microscopy: Advances in Scientific Research and Education*; Méndez-Vilas, A., Ed.; Formatex Research Center: Badajoz, Spain, 2014.
23. Bezuidenhout, L.J.; van Dyk, E.E.; Vorster, F.J.; du Plessis, M.C. *On the Characterization of Solar Cells Using Light Beam Induced Current Measurements*; Nelson Mandela Metropolitan University, Centre for Energy Research, Gqeberha, South African, 2012.
24. Breitenstein, O.; Bauer, J.; Bothe, K.; Hinken, D.; Müller, J.; Kwapil, W.; Schubert, M.C.; Warta, W. Luminescence imaging versus lock-in thermography on solar cells and wafers. In Proceedings of the 26th European Photovoltaic Solar Energy Conference and Exhibition, Hamburg, Germany, 5–6 September 2011; pp. 1031–1038.
25. Hu, Y.; Cao, W.; Wu, J.; Ji, B.; Holliday, D. Thermography-based virtual MPPT scheme for improving PV energy efficiency under partial shading conditions. *IEEE Trans. Power Electron.* **2014**, *29*, 5667–5672.
26. Hu, Y.; Cao, W.; Ma, J.; Finney, S.J.; David Li, D. Identifying PV module mismatch faults by a thermography based temperature distribution analysis. *IEEE Trans. Device Mater. Reliab.* **2014**, *14*, 951–960.